Passive Scalar Transport in Polymer Drag-Reduced Turbulent Channel Flow

V. K. Gupta, R. Sureshkumar, and B. Khomami
Dept. of Chemical Engineering, Washington University, St. Louis, MO 63130

DOI 10.1002/aic.10465
Published online May 4, 2005 in Wiley InterScience (www.interscience.wiley.com).

Passive scalar transport in turbulent channel flow of viscoelastic dilute polymer solutions exhibiting drag reduction (DR) is studied using direct numerical simulations for DR values up to 74.0%. DR is accompanied by the stabilization of low-speed streaks in the buffer layer that are primarily responsible for the streamwise heat transport. Moreover, as DR increases, the Reynolds stress and the root mean square fluctuations in the wall-normal and spanwise velocity components decrease. Thus, as DR is increased, streamwise heat flux increases, whereas both wall-normal and spanwise heat fluxes decrease. Consequently, for large DR values, the flow acts as a highly efficient heat pump. The turbulent Prandtl number, defined as the ratio of the eddy diffusivities of momentum to heat, increases from its Newtonian limit of unity to a value that exceeds the molecular Prandtl number for DR = 74.0%. This experimentally well documented phenomenon is predicted using first-principle simulations for the first time in this work. © 2005 American Institute of Chemical Engineers *AIChE J,* 51: 1938–1950, 2005
Keywords: turbulent drag reduction, heat transfer reduction, viscoelastic, FENE-P, passive scalar

Introduction

The transport of heat in turbulent flows is a central concern in process design. Turbulent flow field causes fluctuations in a scalar field, such as temperature or concentration, by turbulent convection. In turn these fluctuations could influence the velocity field through mean gradients and/or variation in density and viscosity. However, if the temperature or concentration gradient is small the influence of the scalar field on the velocity can be neglected. In this limit, the transport of the scalar is considered passive, that is, the scalar field and turbulent velocity fields are decoupled. Consequently, the transport of the scalar can be determined independently by solving the appropriate conservation equation for a given turbulent velocity field. The latter is typically obtained from direct numerical simulation (DNS) in which the conservation laws of mass and momentum are solved without invoking ad hoc closure approximations. For example, the procedure described above has been used to determine scalar transport in Newtonian turbulent flows.[1] In this article, we report—for the first time—DNS results illustrating the effect of polymer-induced turbulent drag reduction (DR) on the turbulent transport characteristics of a passive scalar in plane channel flows.

Polymer-induced drag reduction refers to the dramatic (up to 70%) reduction in turbulent friction factor accomplished by the addition of small amounts of high molecular linear polymers [such as polyethylene oxide (PEO), polyacrylamide, polymethylmethacrylate] to the turbulent pipe/channel flow of a Newtonian solvent. Since its discovery in the 1940s,[2,3] the influence of the additives on turbulent statistics and structure has been extensively investigated in pipe, channel, and boundary-layer flows.[4-10] These studies have also demonstrated several flow modifications accompanying DR, such as the damping of fluctuations of the velocity normal to the wall surface, enhancement of the streamwise velocity fluctuations, and an increase in the spacing between low-speed streaks in the buffer layer.

Two main mechanisms of polymer-induced drag reduction have been proposed based on the experimental observations. The first mechanism is based on the fact that polymer molecules undergo a coil-to-stretch transition, causing an increase in

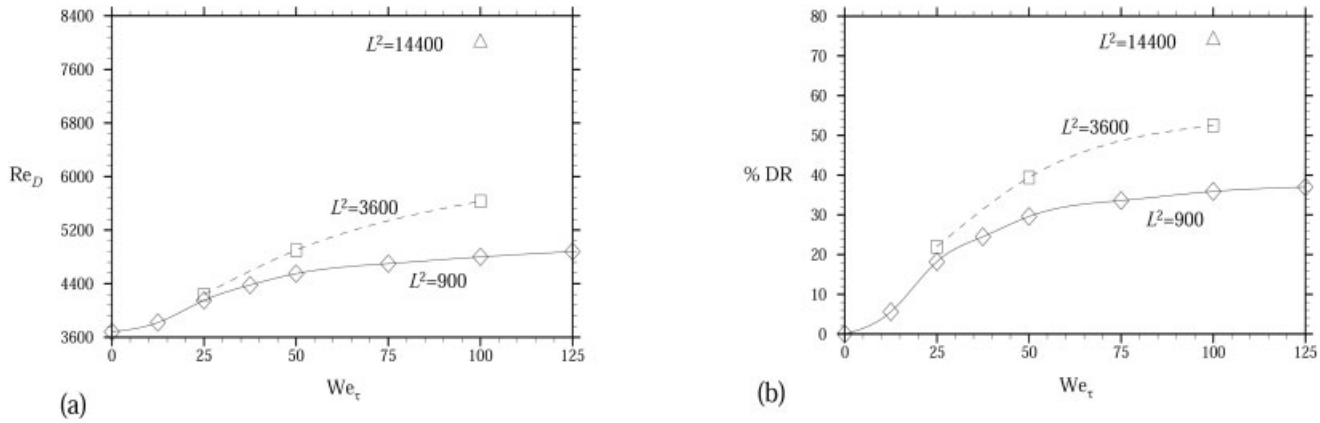

Figure 1. Variation of (a) the mean flow Reynolds number (Re_D) and (b) percentage drag reduction (%DR) as a function of We_τ.

the elongational viscosity of the solution leading to the suppression of Reynolds stress–producing events.[6,11] The second mechanism assumes that coil-to-stretch transition is not possible in channel or pipe flows with constant cross section; rather, drag reduction is associated with the storage of elastic energy in the polymer molecules and the resulting disruption of the energy cascade.[12] Direct numerical simulations of viscoelastic turbulent channel flow using kinetic theory–based models have identified that the enhancement in extensional viscosity caused by flow-induced chain stretching is a key characteristic of drag-reducing fluids.[13-18] The increased extensional viscosity has been found to stabilize the quasi-streamwise vortices in the buffer layer whose lift up and fragmentation are responsible for the production of the bulk of the Reynolds stress.[19-21]

One of the technological applications of drag-reducing additives is to reduce the pumping power required for circulating water in district heating and cooling (DHC) systems. However, when applying drag-reducing additives to a DHC system a heat-transfer problem is inevitably encountered because the heat flux in the wall-normal direction of a drag-reducing flow is also significantly reduced because of the suppression of turbulence. For example, for a 200 ppm polyacrylamide solution at an apparent Reynolds number of 3×10 exhibiting approximately 70% DR, a 90% heat-transfer reduction (HTR) is reported.[22] Early heat-transfer experiments with drag-reducing fluids showed that the heat transfer coefficient is reduced at a rate faster than the accompanying reduction in friction factor.[23,24] More recent experiments have also shown this trend.[22] An analogous reduction in heat-transfer rate is observed in the case of drag-reducing surfactant solutions.[25]

Several attempts to enhance the heat-transfer efficiency of drag-reducing flow by additives have appeared in the literature.[25,26] For example, Li et al.[26] showed that the suppression in turbulence in drag-reducing surfactant solution is a result of the networks of rodlike micelles in the surfactant solutions and any activity that could destroy these networks would result in the elimination of drag reduction and prevent HTR. Nevertheless, the trade-off between the HTR and DR in industrial applications has not been adequately resolved. Furthermore, the mechanism of the HTR itself in drag-reduced flows has not been clearly established.

In this study the turbulent transport of a passive scalar in a viscoelastic turbulent channel flow is examined by directly solving the unsteady, three-dimensional equations for mass and momentum conservation, viscoelastic stress evolution, and passive scalar transport. Specifically, we consider the temperature field as our passive scalar. Clearly our results are also applicable to turbulent mass transfer (that is, the thermal diffusivity, heat flux, and the Prandtl number in the heat transfer problem should be replaced with mass diffusivity, mass flux, and the Schmidt number, respectively).

The paper is organized as follows. In the following section we present the governing equations and the numerical procedures, followed by results and discussion. Conclusions are presented in the final section.

Governing Equations and Numerical Procedures

For the channel Poiseuille flow considered in this study, we chose the x-axis as the mean flow direction, that is, the direction of the constant, externally imposed, pressure gradient and the y- and the z-axes as the wall-normal and spanwise directions, respectively. We denote the zero-shear kinematic viscosity as ν_0, defined as the ratio of total zero-shear viscosity μ_0, to the density of the polymer solution ρ. We use the friction velocity, defined as $U_\tau = \sqrt{\tau_w/\rho}$, as the velocity scale, where τ_w represents the shear stress at the wall, ν_0/U_τ is the length scale, and ν_0/U_τ^2 is the timescale. Using these scales the dimensionless equations for the conservation of momentum and mass are given as follows

$$\frac{\partial \tilde{\boldsymbol{v}}}{\partial t} + \tilde{\boldsymbol{v}} \cdot \boldsymbol{\nabla} \tilde{\boldsymbol{v}} = -\boldsymbol{\nabla} \tilde{p} + [\beta \boldsymbol{\nabla}^2 \tilde{\boldsymbol{v}} + (1-\beta) \boldsymbol{\nabla} \cdot \tilde{\mathbf{T}}] + \frac{1}{\mathrm{Re}_\tau} \mathbf{e}_x \quad (1)$$

$$\boldsymbol{\nabla} \cdot \tilde{\boldsymbol{v}} = 0 \quad (2)$$

where $\tilde{\boldsymbol{v}} = (\tilde{u}, \tilde{v}, \tilde{w})$, $\tilde{p}$ and $\tilde{\mathbf{T}}$ denote the instantaneous values of the velocity, the excess pressure, and the viscoelastic contribution to the total stress, respectively. The pressure is scaled by the wall shear stress τ_w. The last term in Eq. 1 represents the constant, mean pressure drop per unit length across the channel, which in the dimensionless units used here is represented by the inverse of the friction Reynolds number $\mathrm{Re}_\tau \equiv hU_\tau/\nu_0$,

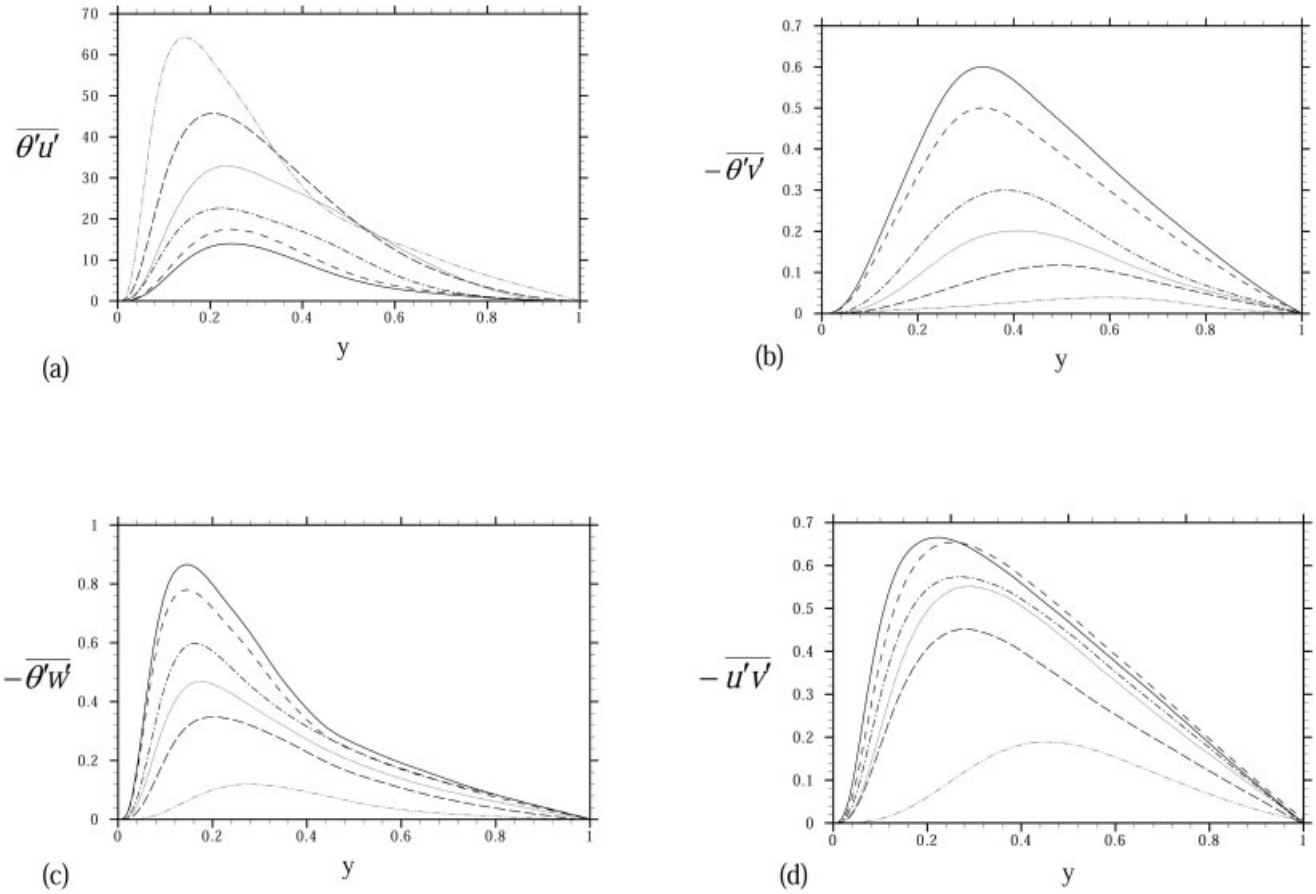

Figure 2. Variation of (a) the streamwise heat flux ($\overline{\theta' u'}$), (b) the normal heat flux ($-\overline{\theta' v'}$), (c) the spanwise heat flux ($-\overline{\theta' w'}$), and (d) the Reynolds shear stress ($-\overline{u' v'}$) as a function of distance from the wall for %DR = 0 (solid line), 5.6 (dashed line), 18.2 (dashed dot line), 29.6 (dotted line), 37.0 (long dashed line), and 74.0 (dashed dot dot line).

where h is the channel half-width. The parameter β appearing in Eq. 1 represents the ratio of the solvent (μ_s) to the total zero-shear rate solution viscosity (μ_0). Finally, note that the viscoelastic stress tensor $\tilde{\mathbf{T}}$ is made dimensionless using a viscous stress scaling, that is, $\mu_{p0} U_\tau^2/\nu_0$, where $\mu_{p0} = \mu_0 - \mu_s$ is the polymer contribution to the total zero-shear solution viscosity.

Equations 1 and 2 are supplemented by a closed-form constitutive equation for the viscoelastic stress contribution. The closed-form constitutive equation used is the FENE-P (finitely extensible nonlinear elastic–Peterlin) dumbbell model. In this model, a polymer chain is represented by a dumbbell consisting of two beads representing the hydrodynamic resistance connected by a finitely extensible entropic spring. The viscoelastic stress $\tilde{\mathbf{T}}$ is related to the departure of the conformation tensor $\tilde{\mathbf{c}}$, characterizing the average second moment of the polymer chain end-to-end distance vector, from its equilibrium unit isotropic tensor state $\mathbf{1}$, as

$$\tilde{\mathbf{T}} = \frac{\tilde{f}\tilde{\mathbf{c}} - \mathbf{1}}{\mathrm{We}_\tau} \tag{3}$$

where $\mathrm{We}_\tau = \lambda U_\tau^2/\nu_0$ is the Weissenberg number, λ is the polymer relaxation time, and

$$\tilde{f} = \frac{L^2 - 3}{L^2 - \mathrm{trace}(\tilde{\mathbf{c}})} \tag{4}$$

where L^2 is the square of the dimensionless (average) maximum extensibility, that is, $\mathrm{trace}(\tilde{\mathbf{c}}) \le L^2$. Note that $\tilde{\mathbf{c}}$ and L^2 are made dimensionless with respect to kT/H^*, where k, T, and H^* denote the Boltzmann constant, the absolute temperature, and the (Hookean) dumbbell spring constant, respectively.

The evolution equation for the conformation tensor $\tilde{\mathbf{c}}$ is given by[27]

$$\frac{\partial \tilde{\mathbf{c}}}{\partial t} + \tilde{\boldsymbol{v}} \cdot (\boldsymbol{\nabla} \tilde{\mathbf{c}}) - [\tilde{\mathbf{c}} \cdot (\boldsymbol{\nabla} \tilde{\boldsymbol{v}}) + (\boldsymbol{\nabla} \tilde{\boldsymbol{v}})^T \cdot \tilde{\mathbf{c}}] = -\frac{\tilde{f}\tilde{\mathbf{c}} - \mathbf{1}}{\mathrm{We}_\tau}. \tag{5}$$

Equations 1–5, along with the no-slip boundary conditions for the velocity on the channel walls, constitute the governing equations for the viscoelastic channel flow, which are subsequently solved numerically.

The choice of the FENE-P model has been motivated by the fact that it can predict the rheological properties of dilute solutions of high molecular weight polymers such as aqueous solutions of PEO used extensively in experimental studies of polymer-induced turbulent DR with reasonable accuracy.

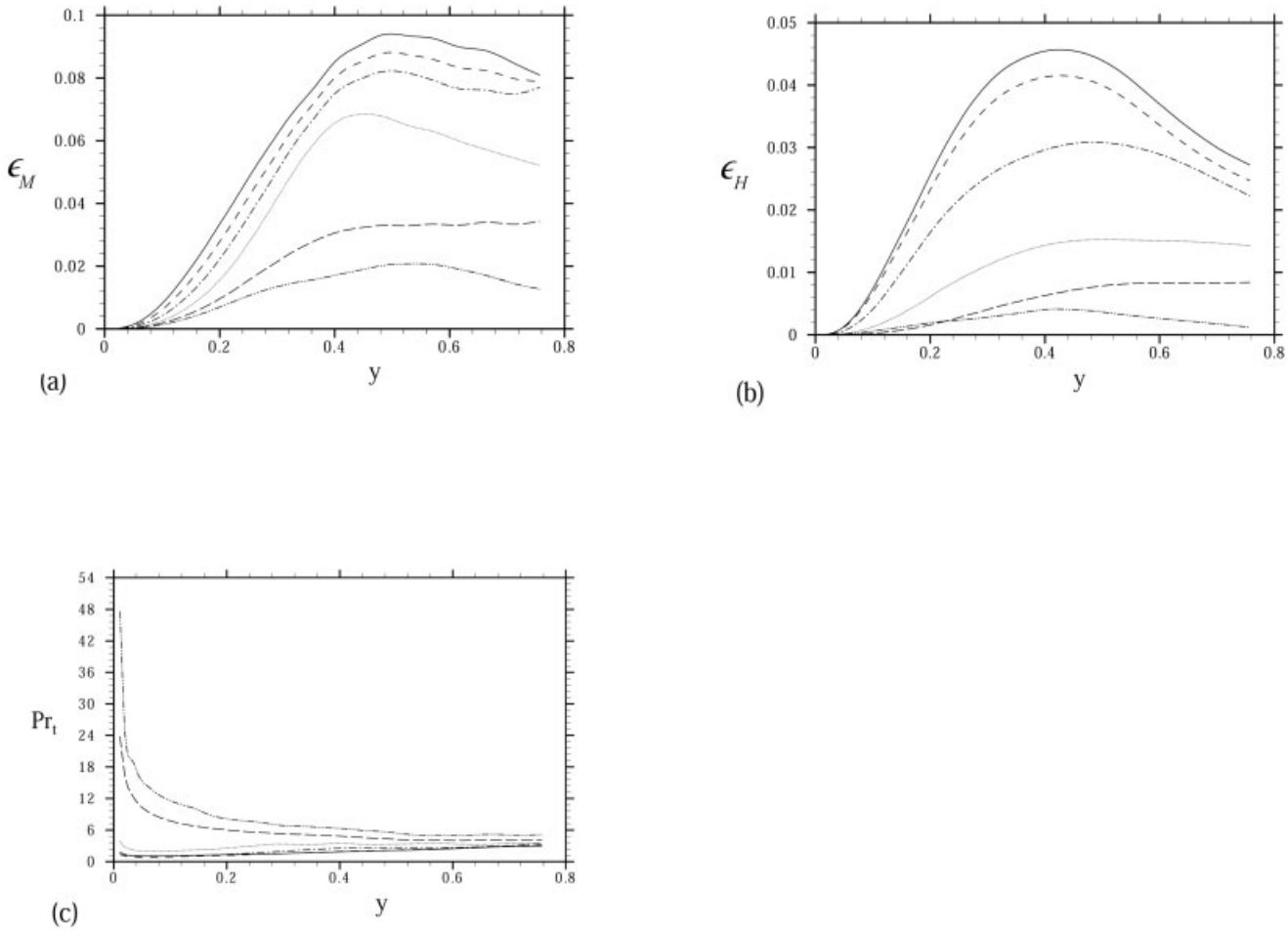

Figure 3. Variation of (a) eddy diffusivity of momentum (ε_M), (b) eddy diffusivity of heat (ε_H), and (c) turbulent Prandtl number as a function of distance from the wall for %DR = 0 (solid line), 5.6 (dashed line), 18.2 (dashed dot line), 29.6 (dotted line), 37.0 (long dashed line), and 52.5 (dashed dot dot line).

Moreover, prior DNS studies using this model have been able to qualitatively describe the DR phenomenon and the accompanying flow modifications.[13,16-18]

The numerical algorithm used for the time integration of Eqs. 1–5 can be found in Dimitropoulos et al.[14] and other studies.[28,29] Recent computations by Housiadas and Beris[16] have shown that the extent of DR is relatively insensitive to Re_τ ($125 \leq \mathrm{Re}_\tau \leq 590$) for fixed We_τ and L^2. Thus, we have performed simulations at a single Re_τ value (that is, 125). Simulation domains of dimensions $10h \times 2h \times 5h$ for $L^2 =$ 900, 3600, and $40h \times 2h \times 5h$ for $L^2 = 14{,}400$ in the x-, y-, and z-directions, respectively, are used. The streamwise (x) dimension of the domain is chosen to be the largest to capture the elongated quasi-streamwise vortical structures. The simulations reported in this work were performed with 64 (in x) $\times$ 65 (in y) $\times$ 64 (in z) mesh for $L^2 = 900$, 3600, and 256 (in x) $\times$ 65 (in y) $\times$ 64 (in z) for $L^2 = 14{,}400$ for $\mathrm{Re}_\tau = 125$, which is adequate to obtain mesh-converged turbulent statistics.[13,21] The streamwise (x) mesh resolution is chosen to maintain the same spatial resolution as the domain size is enhanced to capture the very elongated vortical structures observed at high %DR. In the two periodic directions, x, z, Fourier representations were used, whereas in the nonhomogeneous wall-normal direction, a Chebyshev approximation was used. The (dimensional) time-step size Δt, used in the viscoelastic simulations, is typically $10^{-4}h/U_\tau$, whereas in the Newtonian case it is $10^{-3}h/U_\tau$. The friction Reynolds numbers $\mathrm{Re}_\tau = 125$ corresponds to mean flow Reynolds numbers based on the channel height (Re_m) of 3680 for the Newtonian flow. The simulations reported in this work were performed on 64-bit DEC-alpha 667-MHz 4MB L3 Cache 2-GB RAM LINUX workstations. Typical CPU time for one eddy turnover time is 2 days.

There are three parameters that influence percentage DR: (1) the fluid relaxation time characterized by We_τ, (2) molecular flexibility signified by L^2, and (3) the parameter β appearing in Eq. 1. The mean flow Reynolds number Re_D, based on hydraulic diameter defined as twice the ratio of cross section of the stream to the wetted perimeter, and percentage DR vs. We_τ for $L^2 = 900$, 3600, 14,400 and $\beta = 0.9$ are shown in Figures 1a and 1b. It can be seen that for a given value of L^2 percentage DR increases with increasing We_τ and eventually asymptotes. However, a larger percentage DR can also be accomplished by increasing L^2 for a fixed value of We_τ as depicted in Figure 1b. We_τ values used in this study range between 6.25 and 125. For the FENE-P fluid with $L^2 = 900$ and $\beta = 0.9$, the onset of DR occurs for $\mathrm{We}_\tau \approx 6.25$, whereas for $\mathrm{We}_\tau = 125$ a DR of 37%

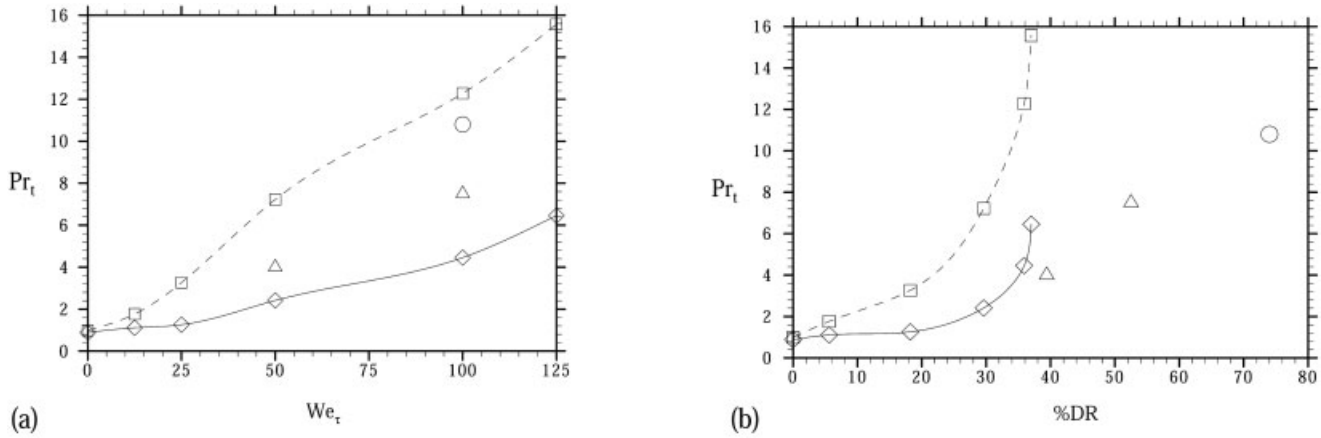

Figure 4. Variation of turbulent Prandtl number (Pr_t) as a function of (a) We_τ, (b) %DR in the buffer layer ($y^+ = 14.6$) for (L^2, Pr) = (900, 6) (◇), (3600, 6) (△), (14,400, 6) (○), and (900, 15) (□).

is seen.[16,18] The highest DR of 74.0% reported in this work is obtained for $L^2 = 14{,}400$ and $We_\tau = 100$. It should be noted that this value corresponds to the maximum drag-reduction asymptote or the Virk asymptote at this Re_τ.[7]

Once the velocity field is obtained for each time step, the corresponding scalar field is obtained by integrating the following conservation equation for the temperature field:

$$\frac{\partial \tilde{\theta}}{\partial t} + \tilde{\boldsymbol{v}} \cdot \boldsymbol{\nabla} \tilde{\theta} = \frac{1}{\mathrm{Re}_\tau \mathrm{Pr}} \boldsymbol{\nabla}^2 \tilde{\theta} + Q \tag{6}$$

where $\tilde{\theta}$ represents the instantaneous temperature; Pr denotes the molecular Prandtl number, defined as the ratio of kinematic viscosity to thermal diffusivity; and Q represents a source term. The following initial and boundary conditions were used while solving the above scalar transport equation using a fully spectral algorithm that uses Chebyshev polynomials in the wall-normal direction and Fourier series in periodic directions:

$$\tilde{\theta}(x, y, z, 0) = 0.5(1 - y^2)$$
$$\tilde{\theta}(x, -1, z, t) = 0 \qquad \tilde{\theta}(x, 1, z, t) = 0 \tag{7}$$

with $Q = 2/(\mathrm{Re}_\tau \mathrm{Pr})$. The above boundary conditions suggested by Moin and Kim[1] are well suited for implementation in simulation with periodic directions. They represent the physical situation in which heat is created internally and removed from both walls.

Results and Discussion

Results are reported for $L^2 = 900$, 3600, and 14,400 and $\beta = 0.9$. Water (Pr = 6) is chosen as the medium in the present study, although we have performed another set of calculations for Pr = 15 to ensure the robustness of the results. For any flow variable $\tilde{u}$, we use the Reynolds decomposition $\tilde{u} = \bar{u} + u'$, where $\bar{u} \equiv \int_{t_i}^{t_i+T} \tilde{u} dt$, where $t_i \le t \le t_i + T$ represents a time interval in the statistically stationary state. Typically, T should be greater than 10 eddy turnover times to obtain meaningful statistics.

Figures 2a–2d show the variation of the streamwise heat flux ($\overline{\theta' u'}$), the normal heat flux ($-\overline{\theta' v'}$), the spanwise heat flux ($-\overline{\theta' w'}$), and the Reynolds shear stress ($-\overline{u' v'}$) as a function of the distance from the channel wall for various values of %DR, respectively. It is seen that as %DR is increased $\overline{\theta' u'}$ is enhanced, whereas $-\overline{\theta' v'}$, $-\overline{\theta' w'}$, and $-\overline{u' v'}$ are decreased. The role that $-\overline{\theta' v'}$ plays in the turbulent production of temperature variance is similar to that of $-\overline{u' v'}$ in the turbulent production of kinetic energy. Figure 3a shows the variation of momentum eddy diffusivity, $\varepsilon_M \equiv -\overline{u' v'}/(d\bar{u}/dy)$, as a function of distance from the channel wall for various values of %DR. It is seen that ε_M increases from zero at the channel wall to a maximum within the core region. Moreover, at any given location within the channel the value of ε_M decreases as %DR is increased. Similar trends are observed for the heat eddy diffusivity, $\varepsilon_H \equiv -\overline{v' \theta'}/(d\bar{\theta}/dy)$ (see Figure 3b). Figure 3c shows the variation of the turbulent Prandtl number, $Pr_t \equiv \varepsilon_M/\varepsilon_H$, as a function of y for the values of %DR reported in Figures 3a and 3b. It is seen that for $0 \le$ %DR ≤ 20, $Pr_t \approx 1$ near the channel wall. However, for larger values of %DR ($\ge$30), near the wall $Pr_t \gg 1$, with the largest value seen for $L^2 = 14{,}400$ at $We_\tau = 100$ corresponding to DR of 74%. For a given value of We_τ, Pr_t decreases as y is increased and eventually asymptotes in the core region. Figures 4a and 4b show the variation of Pr_t as functions of We_τ and %DR,

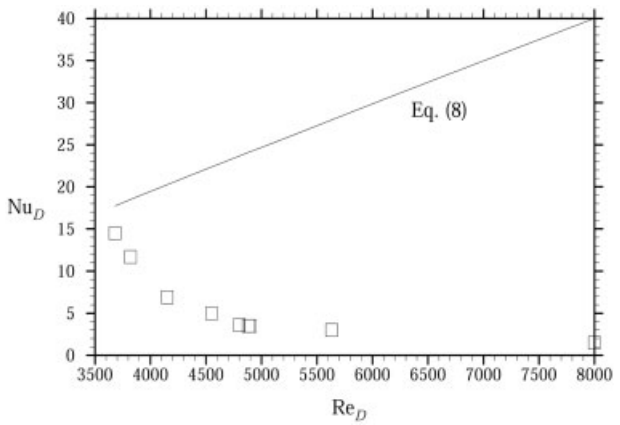

Figure 5. Variation of Nusselt number (Nu_D) as a function of Re_D.

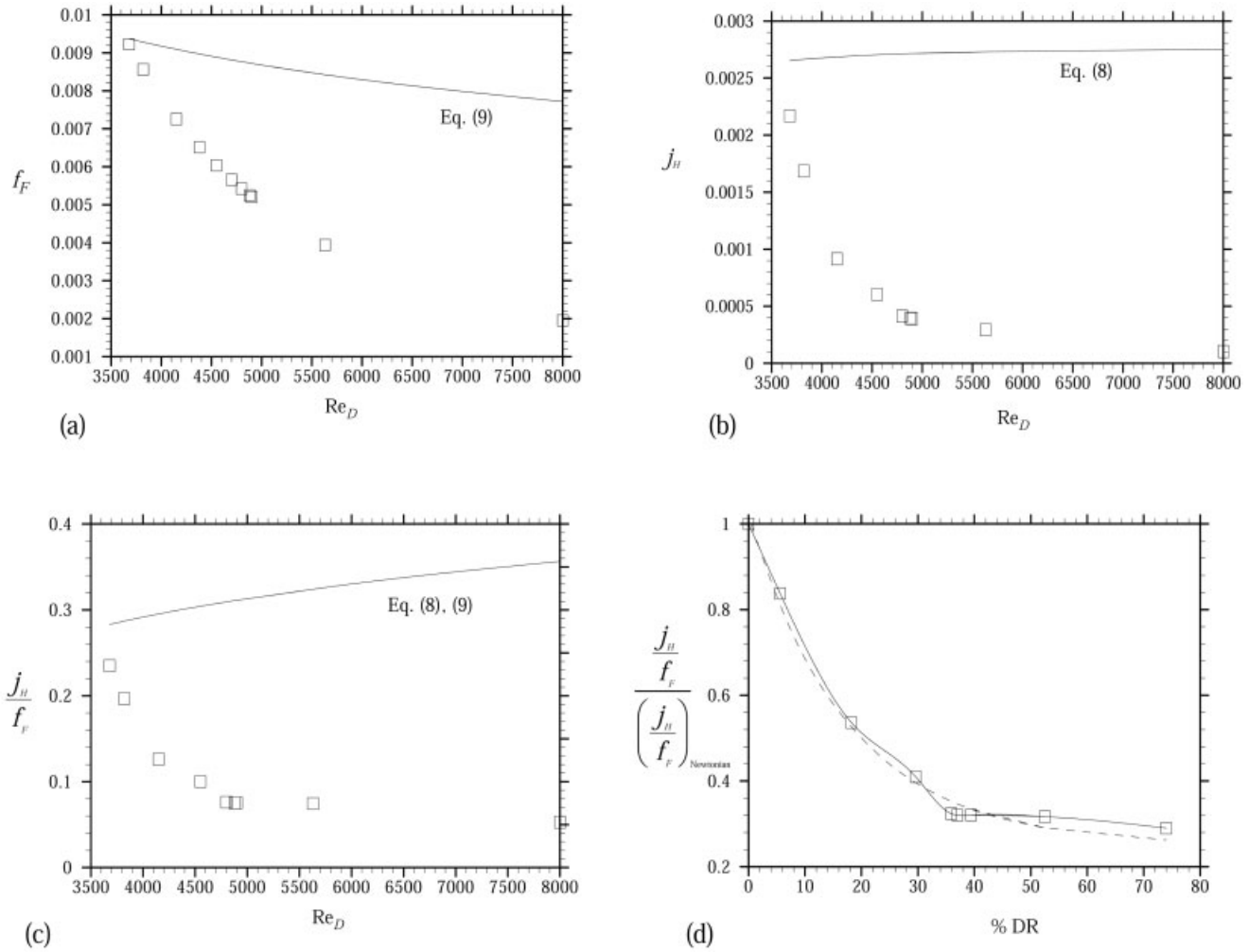

Figure 6. Variation of (a) friction factor (f_F), (b) Colburn factor (j_H), (c) ratio of Colburn factor to friction factor as a function of Re_D, and (d) variation of normalized ratio of Colburn factor to friction factor as a function of %DR.

respectively, in the buffer layer ($y^+ = 14.6$) for two different values of the molecular Prandtl number (Pr = 6 and 15). Once again it can be seen that the turbulent Prandtl number is nearly unity in the buffer layer for lower values of We_τ (%DR). However, for a fixed L^2 as we increase We_τ (and thus %DR) Pr_t increases and attains values that exceed the molecular Prandtl number in the buffer layer, the most active region in a wall-bounded turbulent flow. This is in agreement with experimental observations.[26,30]

It is instructive to compare the DNS results for the heat-transfer coefficient obtained for drag-reduced flows with those predicted by widely used heat-transfer correlations for Newtonian turbulent flows. The heat-transfer coefficient h^*, for turbulent water flow in a smooth channel, can be estimated using the Gnielinski correlation[31]:

$$\mathrm{Nu}_D = 0.012(\mathrm{Re}_D^{0.87} - 280)\mathrm{Pr}^{0.3}\left\{1 + \left(\frac{D}{L}\right)^{2/3}\right\}\left(\frac{\mathrm{Pr}}{\mathrm{Pr}_w}\right)^{0.11} \quad (8)$$

where D is the hydraulic diameter of the channel; L is the length of the channel; $\mathrm{Nu}_D \equiv h^*D/k$ and Re_D, respectively, are the Nusselt and Reynolds numbers based on D; and k is the thermal conductivity of the fluid. The last term in Eq. 8 accounts for the temperature dependency of the properties. Specifically, Pr and Pr_w are the Prandtl numbers calculated at the average fluid temperature and at the wall temperature, respectively. Figure 5 shows the variation of Nu_D as a function of Re_D for the viscoelastic turbulent channel flow corresponding to Figures 1a and 1b. We also plot on the same figure the corresponding values of Nu_D for Newtonian (water) flow obtained from Eq. 8. It is found that in drag-reduced viscoelastic turbulent channel flow Nu_D decreases as Re_D increases, a trend qualitatively opposite to that predicted by the correlation.

Figures 6a–6c show the variation of the Fanning friction factor, $f_F \equiv \tau_w/[(1/2)\rho\langle U\rangle^2]$, the Colburn factor, $j_H = \mathrm{Nu}_D\mathrm{Re}_D^{-1}\mathrm{Pr}^{-1/3}$, and the ratio of the Colburn factor to the friction factor as a function of Re_D, respectively. Also shown in Figure 6a are results for f_F based on Dean's correlation of the friction factor for a Newtonian fluid in a two-dimensional channel:

$$f_F = 0.073\ \mathrm{Re}_D^{-0.25}. \quad (9)$$

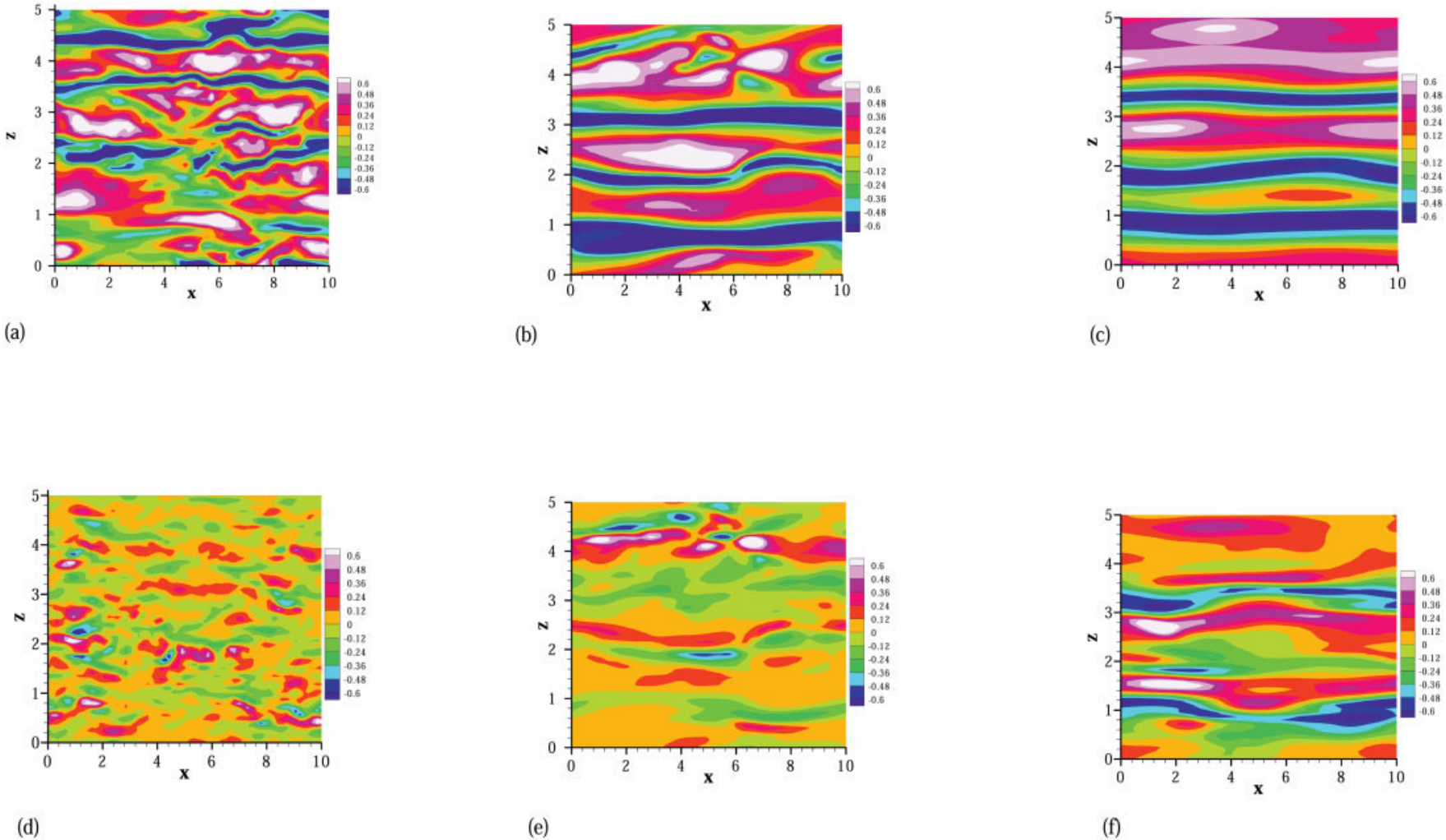

Figure 7. Contours of streamwise velocity fluctuations for (a) %DR = 0, (b) %DR = 37.0, (c) %DR = 52.5, and contours of temperature fluctuations for (d) %DR = 0, (e) %DR = 37.0, and (f) %DR = 52.5 in the (x, z)-plane at $y^+ = 14.6$.

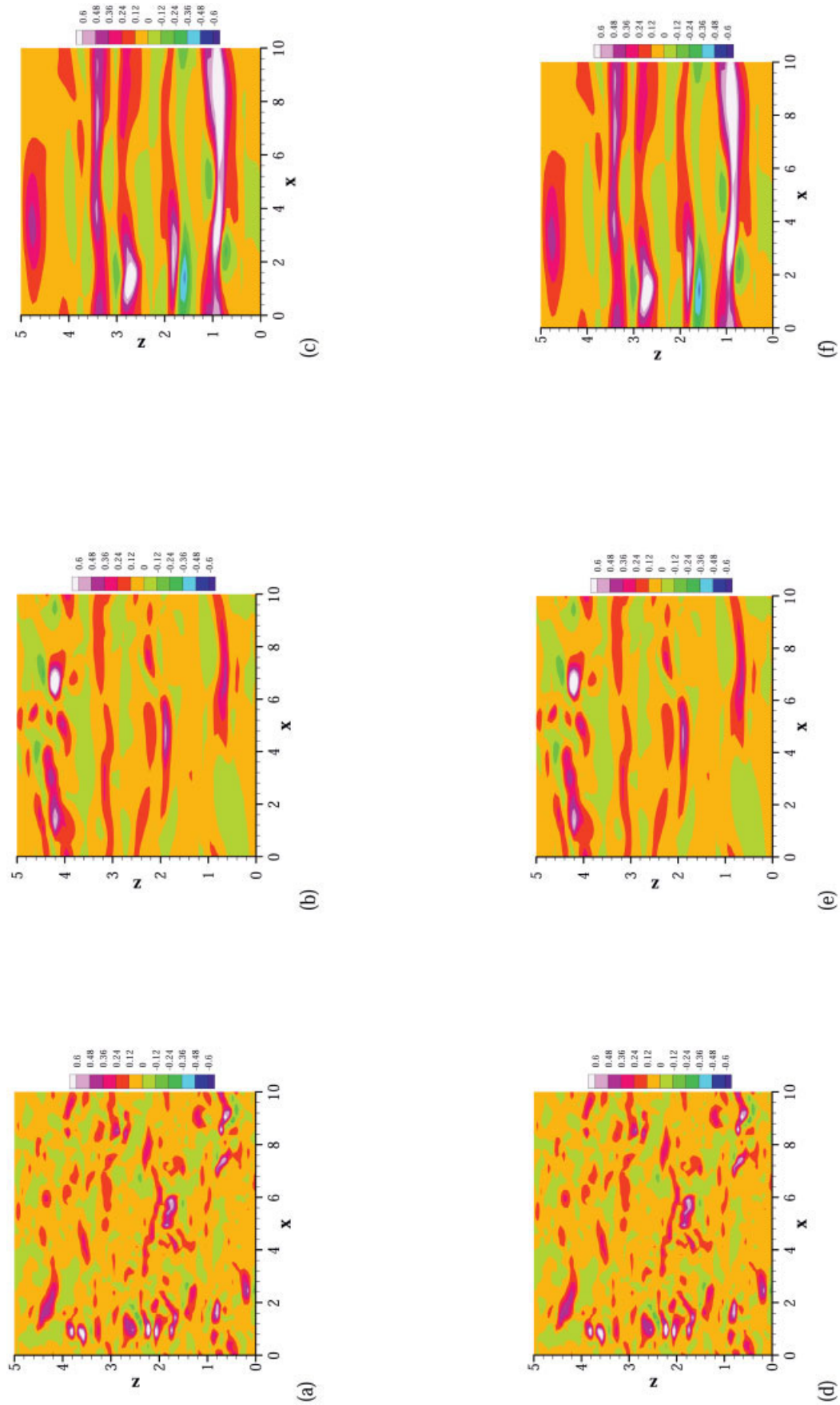

Figure 8. Contours of $u'v'$ for (a) %DR = 0, (b) %DR = 37.0, (c) %DR = 52.5, and contours of $\theta'u'$ for (d) %DR = 0, (e) %DR = 37.0, and (f) %DR = 52.5 in the (x, z)-plane at $y^+ = 14.6$.

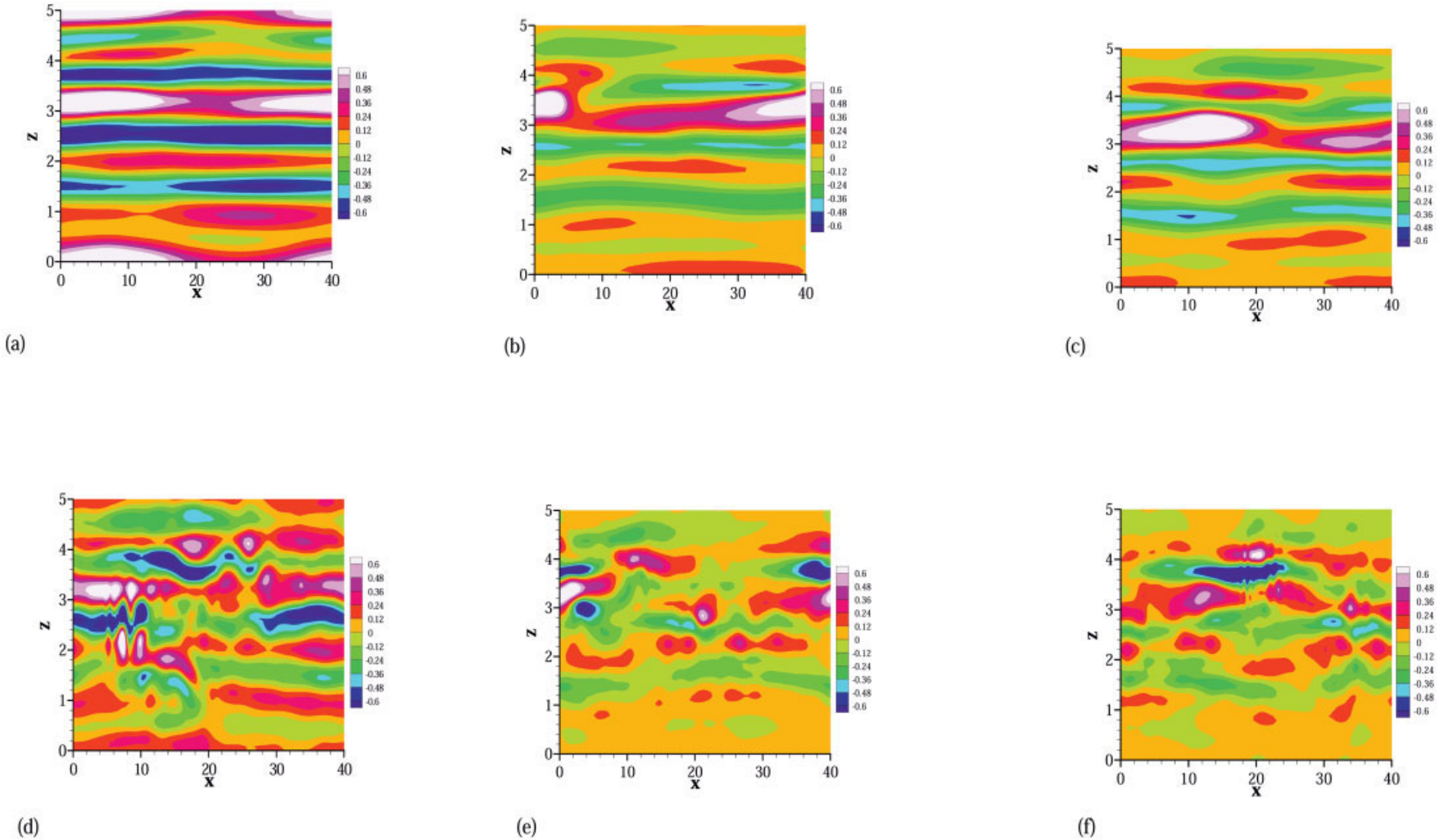

Figure 9. Contours of streamwise velocity fluctuations for %DR = 74.0 at (a) $t = 1h/u_\tau$, (b) $t = 2h/u_\tau$, (c) $t = 3.5h/u_\tau$, and contours of temperature fluctuations for %DR = 74.0 at (d) $t = 1h/u_\tau$, (e) $t = 2h/u_\tau$, and (f) $t = 3.5h/u_\tau$ in the (x, z)-plane at $y^+ = 14.6$.

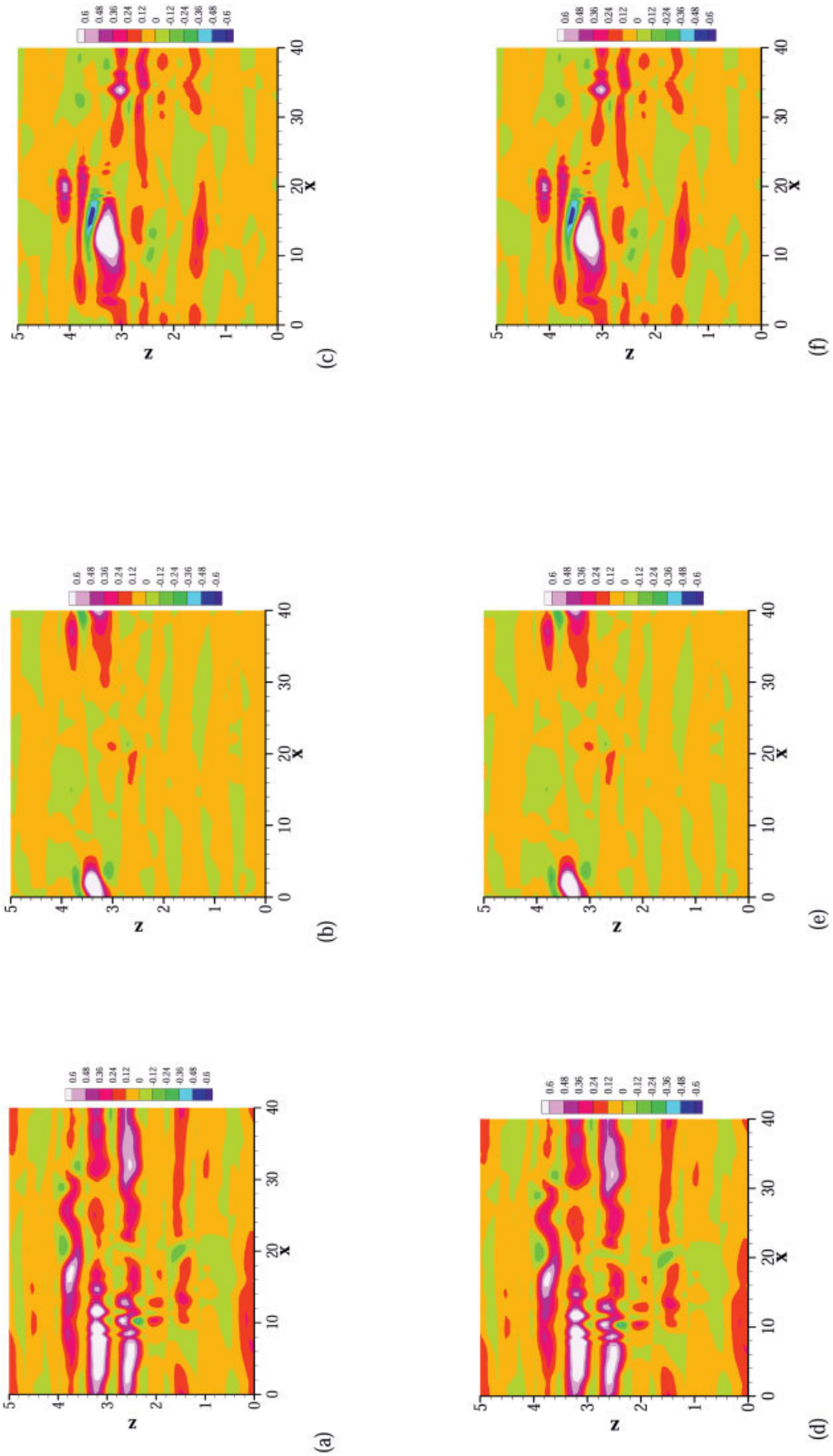

Figure 10. Contours of u′v′ for %DR = 74.0 at (a) $t = 1h/u_\tau$, (b) $t = 2h/u_\tau$, and (c) $t = 3.5h/u_\tau$ and contours of $\theta' u'$ for %DR = 74.0 at (d) $t = 1h/u_\tau$, (e) $t = 2h/u_\tau$, and (f) $t = 3.5h/u_\tau$ in the (x, z)-plane at $y^+ = 14.6$.

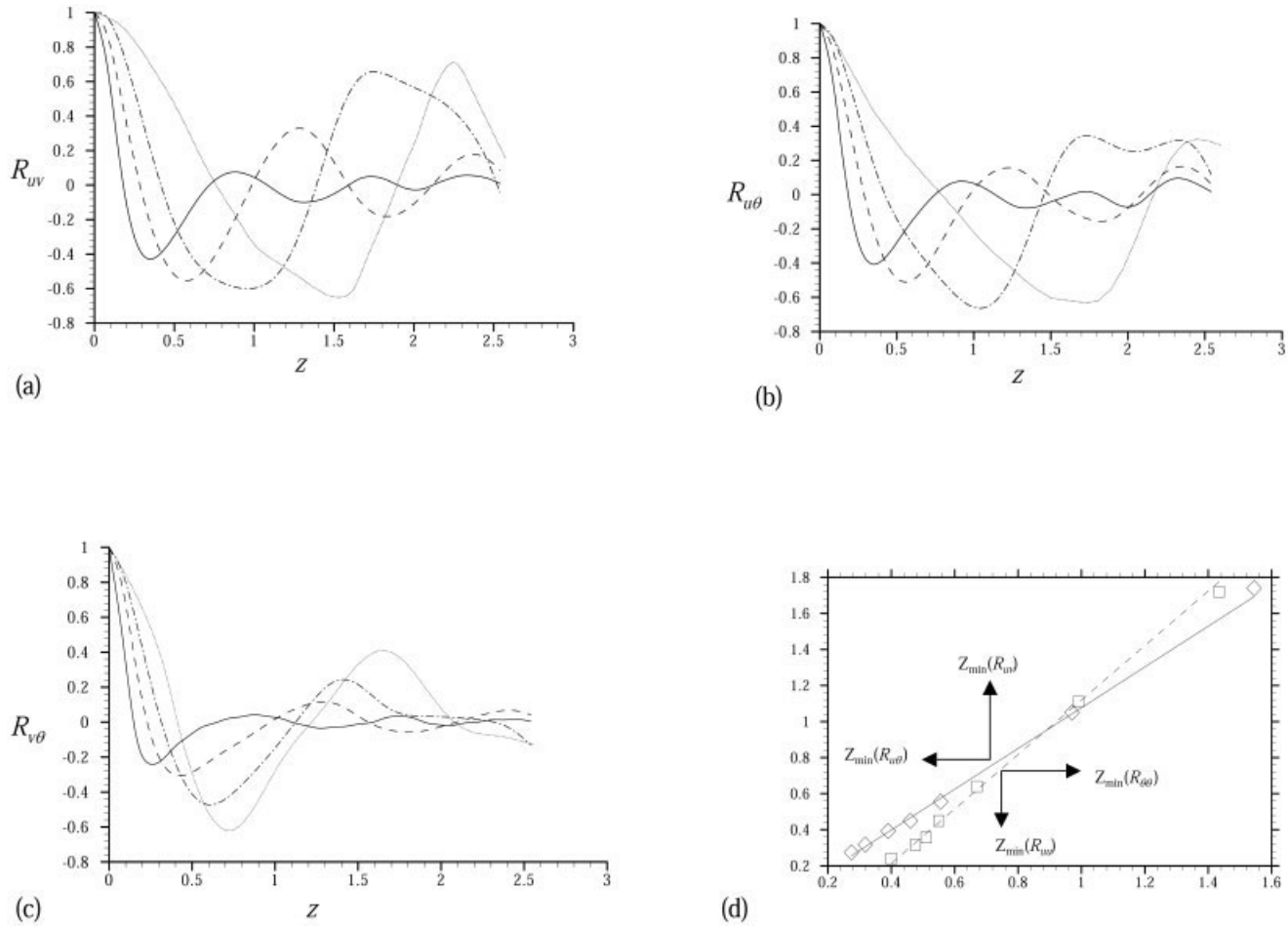

Figure 11. Correlations functions for (a) R_{uv}, (b) $R_{u\theta}$, and (c) $R_{v\theta}$ as a function of spanwise separation at $y^+ = 14.6$ for %DR = 5.6 (solid lines), 37 (dashed lines), 52.5 (dashed dot lines), 74.0 (dotted line); (d) shows variation of location of lowest point in the correlation functions for R_{uv} vs. $R_{u\theta}$ (◇, solid line a linear fit) and R_{uu} vs. $R_{\theta\theta}$ (□, dashed line a linear fit).

Figure 6a shows that for both Newtonian and viscoelastic flows, the friction factor decreases with increasing Reynolds number. Furthermore, for a given Reynolds number, f_F is lower for the viscoelastic flow as a result of DR. The Colburn factor for the Newtonian flow increases slightly with increasing Re_D, whereas for the viscoelastic flow it decreases with increasing Re_D as shown in Figure 6b. Moreover, for a given value of the Reynolds number, j_H for the viscoelastic flow is significantly lower as a result of heat-transfer reduction accompanying DR. Figure 6c shows the ratio of the Colburn factor to the friction factor as a function of Re_D. It is found that this ratio for a Newtonian fluid increases slightly with increasing Reynolds number. However, for a polymeric solution this ratio decreases as Reynolds number (or equivalently %DR) increases. Figure 6d shows the normalized (with respect to the Newtonian value) j_H/f_F as a function of %DR. As %DR increases this ratio decreases to a minimum value of approximately 0.29 at 74.0% DR. We also present a least-square fit of the form $y(x) = y_\infty + c\exp(-\alpha x)$ (with $y_\infty = 0.25$, $c = 0.77$, $\alpha = 0.056$) shown by the dotted line on the same figure where x and y denote %DR and the normalized ratio j_H/f_F, respectively.

To elucidate the mechanism by which heat transfer is modified in drag-reducing flows, we have examined the contour plots of the relevant quantities. Figures 7a–7c show the contour plots of streamwise velocity fluctuations for %DR = 0, 37, and 52.5, respectively, in the (x, z)-plane in the buffer layer ($y^+ = 14.6$). The corresponding contour plots of temperature are shown in Figures 7d–7f. Figures 8a–8c show the contour plots of instantaneous $u'v'$ for %DR = 0, 37, and 52.5, respectively, in the (x, z)-plane in the buffer layer ($y^+ = 14.6$). The corresponding contour plots of $\theta'u'$ are shown in Figures 8d–8f. These contour plots suggest that the axial transport of scalar takes place through the low-speed streaks. It is seen that as %DR increases the streaky structures become more coherent. Further, increasing %DR results in an increase in the streak spacing. Moreover, as MDR is approached the flow becomes highly intermittent. To illustrate this point the contour plots of streamwise velocity for %DR = 74.0 in the (x, z)-plane in the buffer layer ($y^+ = 14.6$) at three different instants of time and the corresponding contour plots of temperature are shown in Figure 9. Figure 10 depicts the contour plots of instantaneous $u'v'$ for %DR = 74.0 in the (x, z)-plane in the buffer layer (y^+

= 14.6) at three different instants of time and the corresponding contour plots of $\theta' u'$. Despite the highly intermittent nature of the flow, it can be clearly observed from Figures 9 and 10 that axial transport of scalar through low-speed streaks is highly facilitated by the tremendous stabilization of low-speed streaks at MDR.

To obtain a more quantitative picture of scalar transport in drag reduced flows, we have evaluated the streak spacing by computing the location of the minimum in the autocorrelation function for velocity fluctuations. Figures 11a–11c show correlation functions for R_{uv}, $R_{u\theta}$, and $R_{v\theta}$, respectively, as a function of spanwise separation in the buffer layer for %DR = 5.6, 37, 52.5, and 74.0. Clearly as drag reduction is enhanced the distance between the z values for which either of these correlations is maximum (at $z = 0$) and a minimum is enhanced. R_{uv} and $R_{u\theta}$ are especially very sensitive to %DR. Moreover, functions R_{uv} and $R_{u\theta}$ follow nearly a similar trend, further verifying that streamwise transport predominantly takes place through the low-speed streaks. Figure 11d shows the variation of the location of lowest point, $Z_{\min}(R_{u\theta})$, in the correlation function for $R_{u\theta}$ as a function of the location of lowest point, $Z_{\min}(R_{uv})$, in the correlation function for R_{uv} for $0 \leq$ %DR ≤ 74.0. We also show a least-square fit (solid line) of the form $Z_{\min}(R_{u\theta}) = mZ_{\min}(R_{uv}) + c$ (with $m = 1.13$, $c = -0.053$) on the same figure. Figure 11d also shows the variation of the location of lowest point, $Z_{\min}(R_{\theta\theta})$, in the correlation function for $R_{\theta\theta}$ as a function of the location of lowest point, $Z_{\min}(R_{uu})$, in the correlation function for R_{uu} for $0 \leq$ %DR $\leq$ 74.0. We also show a least-square fit (dashed line) of the form $Z_{\min}(R_{\theta\theta}) = mZ_{\min}(R_{uu}) + c$ (with $m = 1.51$, $c = -0.391$) on the same figure. The linear fit further underscores the fact that axial heat transfer occurs through the low-speed streaks. In fact, as %DR increases the streaks become very uniform and wall normal and transverse heat fluxes significantly decrease. Thus heat is transported very efficiently axially, similar to that in an efficient heat pump.

Conclusions

Passive scalar transport in turbulent channel flow of viscoelastic dilute polymer solutions exhibiting drag reduction (DR) is studied using direct numerical simulations for DR values up to 74.0%. The influence of We_τ (equivalently %DR) on heat flux, streaks, and the turbulent Prandtl number is examined. It is seen that streamwise heat flux increases with increasing DR as a result of the stabilization of low-speed streaks. However, both wall-normal and spanwise heat fluxes decrease with increasing DR, given that as DR increases the Reynolds stress and the root-mean-square fluctuations in the wall-normal and spanwise velocity components decrease. Furthermore, it is shown that as DR increases the turbulent Prandtl number increases from its Newtonian limit of unity to a value that exceeds the molecular Prandtl number at DR = 74.0%. The reduction and enhancement in the wall-normal and streamwise heat fluxes, respectively, imply that the flow becomes an extremely effective heat pump for large values of DR.

Acknowledgments

The authors acknowledge the financial support provided by DARPA, Grants MDA972-01-1-007 and 29773A.

Literature Cited

1. Kim J, Moin P. Transport of passive scalars in a turbulent channel flow. Proc of 6th Symp on Turbulent Shear Flows, Toulouse, France; 1989:85-96.
2. Toms BA. Some observations of the flow of linear polymer solutions through straight tube at large Reynolds numbers. Proc of the Int Congress on Rheology, 1949 (Vol. 2), Amsterdam: North-Holland; 1949:135-141.
3. Agoston GA, Harte WH, Hottel HC, Klemm WA, Mysels KJ, Pomeroy HH, Thompson JM. Flow of gasoline thickened by napalm. *Ind Eng Chem*. 1954;46:1017-1021.
4. Metzner AB, Park MG. Turbulent flow characteristics of viscoelastic fluids. *J Fluid Mech*. 1964;20:291-303.
5. Hershey HC, Zakin JL. A molecular approach to predicting the onset of turbulent drag reduction in the turbulent flow of dilute polymer solutions. *Chem Eng Sci*. 1967;22:1847-1857.
6. Lumley JL. Drag reduction by additives. *Annu Rev Fluid Mech*. 1969;1:367-384.
7. Virk PS. Drag reduction fundamentals. *AIChE J*. 1975;21:625-656.
8. Blackwelder RF, Kaplan RE. On the wall structure of the turbulent boundary layer. *J Fluid Mech*. 1976;76:89-112.
9. Luchik TS, Tiederman WG. Turbulent structure in low-concentration drag-reducing channel flows. *J Fluid Mech*. 1988;190:241-263.
10. Walker DT, Tiederman WG. Turbulent structure in a channel flow with polymer injection at the wall. *J Fluid Mech*. 1990;218:377-403.
11. Seyer FA, Metzner AB. Turbulence phenomena in drag-reducing systems. *AIChE J*. 1969;15:426-434.
12. de Gennes PG. Towards a scaling theory of drag reduction. *Physica A*. 1986;140:9-25.
13. Sureshkumar R, Beris AN, Handler RA. Direct numerical simulation of the turbulent channel flow of a polymer solution. *Phys Fluids*. 1997;9:743-755.
14. Dimitropoulos CD, Sureshkumar R, Beris AN. Direct numerical simulation of viscoelastic turbulent channel flow exhibiting drag reduction: Effect of the variation of rheological parameters. *J Non-Newtonian Fluid Mech*. 1998;79:433-468.
15. Dimitropoulos CD, Sureshkumar R, Beris AN, Handler RA. Budgets of Reynolds stress, kinetic energy and streamwise entrophy in viscoelastic turbulent channel flow. *Phys Fluids*. 2001;13:1016-1027.
16. Housiadas KD, Beris AN. Polymer-induced drag reduction: Effects of the variations in elasticity and inertia in turbulent viscoelastic channel flow. *Phys Fluids*. 2003;15:2369-2384.
17. Terrapon VE, Dubief Y, Moin P, Shaqfeh ESG, Lele SK. Simulated polymer stretch in a turbulent flow using Brownian dynamics. *J Fluid Mech*. 2004;504:61-71.
18. Gupta VK, Sureshkumar R, Khomami B. Polymer chain dynamics in Newtonian and viscoelastic turbulent channel flows. *Phys Fluids*. 2004;16:1546-1566.
19. Stone PA, Waleffe F, Gragam MD. Toward a structural understanding of turbulent drag reduction: Nonlinear coherent states in viscoelastic shear flows. *Phys Rev Lett*. 2002;89:208301.
20. Stone PA, Graham MD. Polymer dynamics in a model of the turbulent buffer layer. *Phys Fluids*. 2003;15:1247-1256.
21. Li CF, Gupta VK, Sureshkumar R, Khomani B. Induced turbulent drag reduction: a mechanistic polymeric study. Proc of the XIVth International Congress on Rheology, Seoul, South Korea (2004).
22. Matthys EF. Heat transfer, drag reduction, and fluid characterization for turbulent flow of polymer solutions: Recent results and research needs. *J Non-Newtonian Fluid Mech*. 1991;38:313-342.
23. Cho YI, Hartnett JP. Heat transfer in flows with drag reduction. *Adv Heat Transfer*. 1982;15:59-139.
24. Yoon HK, Ghajar AJ. Heat eddy diffusivity for viscoelastic turbulent pipe flow. *Int Commun Heat Mass Transfer*. 1987;14:237-249.
25. Qi Y, Kawaguchi Y, Lin Z, Ewing M, Christensen RN, Zakin JL. Enhanced heat transfer of drag reducing surfactant solutions with fluted tube-in-tube heat exchanger. *Int J Heat Mass Transfer*. 2001; 44:1495-1505.
26. Li P, Kawaguchi Y, Daisaka H, Yabe A, Hishida K, Maeda M. Heat transfer enhancement to the drag-reducing flow of surfactant solution in two-dimensional channel with mesh-screen inserts at the inlet. *J Heat Transfer*. 2001;123:779-789.
27. Bird RB, Curtiss CF, Armstrong RC, Hassager O. *Dynamics of Polymeric Fluids*. Vol. 2. New York, NY: Wiley; 1987.

28. Sureshkumar R, Beris AN. Effect of artificial stress diffusivity on the stability of numerical calculations and the flow dynamics of time-dependent viscoelastic flows. *J Non-Newtonian Fluid Mech*. 1995;60: 53-80.
29. Beris AN, Sureshkumar R. Simulation of time-dependent viscoelastic channel Poiseuille flow at high Reynolds numbers. *Chem Eng Sci*. 1996;51:1451-1471.
30. Dimant Y, Poreh M. Heat transfer in flows with drag reduction. *Adv Heat Transfer*. 1976;12:77-113.
31. Gnielinski V. New equation for heat and mass transfer in turbulent pipe and channel flow. *Int Chem Eng*. 1976;16:359-367.

Manuscript received Jul. 16, 2004, revision received Oct. 29, 2004, and final revision received Dec. 3, 2004.